HHS Public Access

Author manuscript

Acta Biomater. Author manuscript; available in PMC 2020 July 15.

Published in final edited form as:

Acta Biomater. 2019 July 15; 93: 86–96. doi:10.1016/j.actbio.2019.05.031.

The inclusion of zinc into mineralized collagen scaffolds for craniofacial bone repair applications

Aleczandria S. Tiffany[1], **Danielle L. Gray**[2], **Toby J. Woods**[2], **Kiran Subedi**[2], and **Brendan A.C. Harley**[1,3]

[1]Dept. Chemical and Biomolecular Engineering, University of Illinois at Urbana-Champaign, Urbana, IL 61801

[2]School of Chemical Sciences, University of Illinois at Urbana-Champaign, Urbana, IL 61801

[3]Carl R. Woese Institute for Genomic Biology, University of Illinois at Urbana-Champaign, Urbana, IL 61801

Abstract

Implant osteoinduction and subsequent osteogenic activity are critical events that need improvement for regenerative healing of large craniofacial bone defects. Here we describe the augmentation of the mineral content of a class of mineralized collagen scaffolds under development for craniomaxillofacial bone regeneration via the inclusion of zinc ions to promote osteogenesis *in vitro.* Zinc is an essential trace element in skeletal tissue and bone, with soluble zinc being shown to promote osteogenic differentiation of porcine adipose derived stem cells. We report the development of a new class of zinc functionalized scaffolds fabricated by adding zinc sulfate to a mineralized collagen-glycosaminoglycan precursor suspension that was then freeze dried to form a porous biomaterial. We report analysis of zinc functionalized scaffolds via imaging (scanning electron microscopy), mechanical testing (compression), and compositional (x-ray diffraction, inductively coupled plasma mass spectrometry) analyses. Notably, zinc-functionalized scaffolds display morphological changes to the mineral phase and altered elastic modulus without substantially altering the composition of the brushite phase or removing the micro-scale pore morphology of the scaffold. These scaffolds also display zinc release kinetics on the order of days to weeks and promote successful growth and pro-osteogenic capacity of porcine adipose derived stem cells cultured within these zinc scaffolds. Taken together, we believe that zinc functionalized scaffolds provide a unique platform to explore strategies to improve *in vivo* osteogenesis in craniomaxillofacial bone injuries models.

Keywords

collagen scaffold; zinc; mineral; bone; tissue engineering

Corresponding Author: B.A.C. Harley, Dept. of Chemical and Biomolecular Engineering, Carl R. Woese Institute for Genomic Biology, University of Illinois at Urbana-Champaign, 110 Roger Adams Laboratory, 600 S. Mathews Ave., Urbana, IL 61801, Phone: (217) 244-7112, Fax: (217) 333-5052, bharley@illinois.edu.

1. Introduction

Craniomaxillofacial bone injuries arise from a diverse set of congenital defects as well as oncologic or traumatic injuries. Trauma-related craniomaxillofacial injuries, both those experienced by civilians [1–3] as well as high-energy impact injuries experienced by Warfighters [4, 5], present particular clinical challenges. Trauma-related craniomaxillofacial bone injuries are often large and complex in size and geometry, and cannot be repaired with external fixtures alone[6]. Most often clinical treatment utilizes autografts, bone taken from a secondary site in the patient with the defect, or allografts, bone taken from a human donor [7–9]. Autografts are limited by the size of the defect area as well as concerns associated with secondary site morbidity. Bone allografts raise concerns about disease transmission, rejection, and lot-to-lot variability that may impact graft integration and healing [10]. Thus, there is a clinical need for alternative solutions to address critically sized craniomaxillofacial defects.

Strategies to improve regenerative healing of such bone defects often seek to employ a biomaterial template. The collagen and calcium phosphate mineral nano-crystallites associated with the bone extracellular matrix have inspired a wide range of collagen-mineral composite biomaterials [11–13]. Our laboratory has recently developed a mineralized collagen-glycosaminoglycan scaffold that promotes osteogenesis and mineral deposition *in vitro* without the addition of exogenous factor (e.g. BMP2) [14, 15]. Here, calcium salts added to a suspension of collagen and glycosaminoglycans in phosphorous acid lead to precipitation of a brushite form of calcium phosphate into the collagen network that is subsequently lyophilized to form a porous foam. A portion of the calcium and phosphate ions incorporated into the mineralized scaffolds are released during culture and are believed to accelerate osteogenesis[16]. Craniofacial bones rely on intramembranous ossification processes, and the mineralized collagen scaffold has been previously shown to promote osteogenesis in vitro and also to enhance regenerative healing of craniofacial bone injuries (rabbit calvarial; sub-critical sized porcine mandible) [17–19]. However, as with most tissue engineering biomaterials, the need to enhance osteogenic capacity increases with the size and complexity of craniomaxillofacial trauma. These challenges are heightened given the increasing technical and regulatory challenges associated with the delivery of growth factors to enhance bone healing (e.g., BMP2) [12].

Zinc is an essential trace element found primarily in skeletal tissue and bone [20, 21]. Zinc is an important mediator of bone development and growth. Hojyo *et al.* found that mice with a knockout for Zrt-and Irt-like protein 14 (ZIP14) - a zinc transporter - had shorter long bones and exhibited dwarfism compared to wildtype mice[22]. Similarly, zinc deficiency in humans is related to stunted bone development and dwarfism[23]. *In vitro* studies have shown that zinc ions improve stem cell osteogenesis and increase mineral deposition *in vitro[24,* 25]. Recent work by Bertels *et al.* identified a critical dose range (0.04 – 0.08 mM) of zinc sulfate that when added to osteogenic media enhanced adipose derived stem cell mineral nodule formation in two-dimensional culture [26]. Importantly, the response was biphasic, with zinc sulfate concentrations above 0.08 mM detrimental to cell growth.

In this manuscript we describe the incorporation of zinc into the mineralized collagen scaffold via addition of zinc sulfate into the mineralized collagen suspension prior to lyophilization. We report dose-dependent influences of zinc incorporation on scaffold mechanical and structural properties, composition and organization of scaffold mineral phase, rate of zinc release, and resultant changes in *in vitro* activity of adipose derived stem cells.

2. Materials and Methods

2.1. Scaffold Fabrication

Mineralized collagen-glycosaminoglycan (*Mineralized*) and mineralized collagen-glycosaminoglycan-zinc scaffolds (*Zinc*) were fabricated via lyophilization from mineralized collagen and mineralized collagen zinc precursor suspensions. The mineralized collagen suspension was created as previously described by homogenizing type I collagen (1.9 weight per volume, Sigma Aldrich, St. Louis, Missouri USA), chondroitin-6-sulfate (0.84 weight per volume, Sigma Aldrich), and calcium salts (calcium hydroxide and calcium nitrate, Sigma Aldrich) in mineral buffer solution (0.1456M phosphoric acid/0.037M calcium hydroxide) [16, 27]. The mineralized collagen zinc suspension was prepared in the same manner, with zinc sulfate (Sigma Aldrich) added simultaneously with the calcium salts. Three mineralized collagen zinc scaffold variants were created, inspired by data from a previous study from our group[16] that quantified the release rates of calcium and phosphate ions from mineralized collagen scaffolds. We created three zinc scaffold variants estimated to generate soluble zinc ion concentrations within the scaffold below and above the 0.08mM zinc ion concentration found by Bertels *et al.*[26] to enhance adipose derived stem cell activity in two-dimensional culture. The final zinc scaffold variants contained 0.5 mg/mL (1X Zinc), 2.5 mg/mL (5X Zinc), or 5 mg/mL (10X Zinc) of added zinc sulfate. Precursor suspensions were stored at 4°C and degassed prior to lyophilization.

Scaffolds were subsequently fabricated via lyophilization using a Genesis freeze-dryer (VirTis, Gardener, New York USA) [28]. Briefly, 100uL of precursor suspension was pipetted into each well of a custom 144-well polysulfone mold (6mm diameter, 7mm tall wells). Scaffolds were then fabricated by freezing the suspension via cooling from 20°C to −10°C at a constant rate of 1°C/min followed by a temperature hold at −10°C for 2 hours. The frozen suspension was then sublimated at 0°C and 0.2 Torr, resulting in a porous scaffold network. After fabrication, all scaffolds used for cell culture were sterilized via ethylene oxide treatment for 12 hours utilizing an AN74i Anprolene gas sterilizer (Andersen Sterilizers Inc., Haw River, North Carolina USA) in sterilization pouches [16, 29, 30]. All subsequent handling steps leading to studies of cell activity were performed in a sterile manner.

2.2. Scanning Electron Microscopy and Pore Size Quantification

Dry scaffolds specimens were cut into semi-cylinders and placed on carbon tape, sputter coated with gold/palladium, and imaged using a Philips XL30 ESEM-FEG (FEI Company) at 5kV with a secondary electron detector. Alternatively, critical point drying (CPD) was performed using a Samdri-PVT-3D (Tousimis, Rockville, Maryland USA) to prepare

hydrated and cell-seeded scaffolds prior to SEM imaging [31]. Briefly, scaffolds were placed in formalin for 24 hours and then the aqueous media in hydrated scaffolds was sequentially replaced with ethanol and then liquid CO_2. The specimens were then held above 6.895 kPa and 31°C to remove the CO_2 as a gas with minimal structural deformation.

Quantification of scaffold pore size was performed using a previously described stereology method [32, 33]. Briefly, cylindrical scaffold specimens were embedded in glycomethacrylate (Polysciences Inc., Warrington, Pennsylvania USA) then sectioned (10 μm slices) in both transverse and longitudinal planes. Sections were stained with aniline blue (Thermo Fisher Scientific Inc, Waltham, Massachusetts USA) then imaged using a NanoZoomer Digital Pathology System (Hamamatsu, Japan). A linear intercept macro was then employed to calculate pore size and pore aspect ratio from histology specimens [34, 35].

2.3. X-Ray Diffraction & Unit Cell Analysis

Scaffolds were prepared for x-ray diffraction (XRD) compositional analysis by freeze-drying the mineralized collagen or mineralized collagen zinc precursor suspensions directly in XRD sample holders. Pure zinc sulfate was used as a positive control. Powder XRD data were collected on a Rigaku MiniFlex 600 diffractometer (SN BD63000258–03). Measurements employed Ni-filtered Cu Ka (λ = 1.54178Å) radiation from a copper sealed tube with 40kV voltage and 15mA current in the Bragg-Brentano geometry. Diffraction patterns were measured over the range of 3–100° 2θ by step scanning at a rate of 1s/0.02°. Scaffolds were prepared for unit cell analysis using the same method described above, but with a silicon standard added to each precursor suspension prior to freeze-drying. The silicon standard provided a calibrant to correct the patterns for sample displacement effects. All patterns were corrected and analyzed for comparison of unit cell parameters between scaffold variants, with unit cell refinements performed using TOPAS (Version 4.2. Bruker AXS, Inc., Madison, Wisconsin, USA).

2.4. Quantification of Zn, Ca, and P in freeze-dried scaffolds

Freeze-dried scaffold specimens (samples between 0.5 and 14 milligrams) were analyzed via inductively coupled plasma mass spectrometry (ICP-MS) and inductively coupled plasma optical emission spectrometry (ICP-OES). ICP-MS was used to detect zinc in our scaffolds, while ICP-OES was used to detect calcium and phosphorus. Dry samples were transferred to a digestion tube, then digested with concentrated nitric acid (67–70%) followed by automated sequential microwave digestion in a CEM Mars 6 microwave digester (CEM Microwave Technology Ltd., North Carolina, USA). The final product was a clear aqueous digest which was diluted to a volume of 25mL using DI water. This solution was then introduced to inductively coupled plasma-mass spectrometer (NexION™ 350D ICP-MS, PerkinElmer, USA) for the elemental analysis in a standard mode. Digestion and ICP-MS/ICP-OES analysis parameters are in Supplemental Tables 1–3.

2.5. Zinc Ion Release

The release of zinc ions from mineralized zinc (vs. mineralized) scaffolds was monitored for up to 28 days in culture. Hydrated scaffolds (6mm diameter, 3mm height) were placed in 1

milliliter phosphate buffered saline (PBS) + 1% bovine serum albumin at 37°C for up to 28 days. Aliquots were collected every day for the first 7 days of release followed by every 3 days until day 28, with media replaced after each aliquot collection. Zinc ion release was quantified using ICP-MS. A volume of 0.5mL of the sample was transferred to a digestion tube. Sample degradation and zinc analysis were performed as described above.

2.6. Scaffold Mechanical Properties

Stress-strain curves of the non-hydrated scaffolds were generated using an Instron 5943 mechanical tester (Instron, Norwood, MA) using a 100 N load cell under dry conditions. Samples were compressed at a rate of 2 mm/min with the Young's Modulus determined from the stress-strain curves using conventional analysis methods for low-density open-cell foam structures such as the collagen scaffolds [36–40].

2.7. Porcine Derived Adipose Stem Cell Culture

Primary porcine derived adipose stems cells (pASCs) were used for all *in vitro* cell experiments and were a gift from Dr. Matthew Wheeler (University of Illinois). pASCs were chosen as they have been shown to have robust and well defined osteogenic capabilities [41]; pASCs were also used to identify a dose range of zinc ions to be added into cell culture media (0.04 – 0.08 mM) to enhance osteogenesis. Further, we have previously used a porcine mandibular defect model to evaluate the regenerative capacity of our mineralized collagen scaffolds [18, 26, 41]. Cells were expanded in T175 flasks (Fisher Scientific, Hampton, New Hampshire USA) until passage 6 and cultured in complete mesenchymal stem cell growth media (Low glucose DMEM + L-glutamine, 10% fetal bovine serum, 1% antibiotic-antimycotic) at 37°C and 5% CO_2 until confluent. Once confluent, pASCs were seeded (100,000 cells/scaffold for 7-day experiment, 80,000 cells/scaffold for 56-day experiment) onto mineralized and zinc-functionalized scaffolds using a static seeding method used in our laboratory previously [14, 31, 42]. Cell seeded scaffolds were cultured in mesenchymal stem cell growth media at 37°C and 5% CO2 for up to 56 days (cell activity), with media changed every 3 days.

2.8. Cell Metabolic Activity & Cell Number

The metabolic activity and total cell number in scaffold specimens was measured using alamarBlue and Hoechst assays, respectively, via fluorescent spectrophotometer (Tecan Infinite F200 Pro, Mannedorf, Switzerland). Cell seeded scaffolds were incubated in a 10% alamarBlue solution (Invitrogen, Carlsbad, California USA) for 90 minutes at 37°C under moderate shaking. The active ingredient in the alamarBlue reagent, resazurin, is reduced to a compound that is highly fluorescent when added to metabolically active cells[16, 43]. The relative cell metabolic activity was determined from a standard curve generated with known pASC concentrations and reported as a fraction of initial seeding cell count and normalized by the initial seeding density (i.e. experimental value of 1 indicate the metabolic activity of the number of cells originally seeded onto the scaffold). The total number of pASCs within a scaffold specimen was quantified via a Hoechst assay. Briefly, cell-seeded scaffolds were rinsed in PBS to remove dead, unattached cells[33] then digested in papain (4.8 mg/mL, Sigma Aldrich) at 60°C for 18–24 hours. Lysates were then incubated with Hoechst 33258 dye (Invitrogen) to fluorescently label double-stranded DNA that could be quantified via a

fluorescent spectrophotometer, then translated into cell count through a standard curve of known pASC numbers.

2.9. RNA Isolation and Gene Expression Characterization

RNA was isolated from scaffolds using 1% beta-mercaptoethanol lysis solution and the RNeasy Plant Mini Kit (Qiagen, Venlo, Netherlands), then was reverse transcribed using a QuantiTect Reverse Transcription Kit (Qiagen) and a BioRad S1000 thermal cycler (BioRad, Hercules, California USA). Real-time PCR reactions were carried out in duplicate, using 10 ng of cDNA and either QuantiTect SYBR Green (BioRad) or Taqman (ThermoFisher, Waltham, Massachusetts USA) primers. Primers were chosen because they're validated for both selectivity and efficiency during PCR; however, the difficulty in finding validated primers for all targets in porcine cells with one system led to the use of both SYBR Green and Taqman systems. A Quantitect SYBR green PCR kit (Qiagen) or Taqman PCR kit (ThermoFisher) – depending on primer type – along with an Applied Biosystems 7900HT Fast Real-Time PCR System was used to perform the real-time PCR. Glyceraldehyde 3-phosphate dehydrogenase (GAPDH) was used as a housekeeping gene, with both Taqman and SYBR green primers for GAPDH used to compare between primer types. Gene expression profiles were obtained for Collagen 1 (Col1A), osteocalcin (OCN), bone morphogenic protein 2 (BMP2), transcription factor Sp7 (Osterix), runt-related transcription factor 2 (RunX2), zinc transporter 7 (ZnT7), Zrt- and Irt-like protein 1 (ZIP1), and ZIP13 (Table 1). Taqman primers (ThermoFisher) were used for Col1A, OCN, BMP2, Osterix, and ZnT7 while SYBR green primers (BioRad) were used for RunX2, ZIP1, and ZIP13.

2.10. Micro Computed Tomography

The mineral content of mineralized collagen vs. mineralized collagen zinc scaffolds was assessed via micro-computed tomography (micro-CT). Cell-seeded and unseeded control scaffolds were examined after 28 and 56 days in culture and compared to an unseeded control scaffold (day 0). All samples were fixed in 10% formalin (Polysciences, Warrington, Pennsylvania USA), with scans performed using a MicroXCT-400 (Zeiss, Oberkochen, Germany). Scans consisted of 721 images performed at 40 kV and 8 watts. Total particle count and particle size (area) were obtained using the "analyze particles" function in ImageJ. Image stacks were imported into ImageJ, converted to 16-bit binary images, and converted into black and white images using the Shanbhag automatic thresholding method [44, 45]. Within the analyze particles settings, we set the particle size as "0-Infinity" (pixels^2; ~364 pixel is 6mm) and circularity as "0.00–1.00." This allows the counting of particles at any size and any circularity (i.e. shapes other than spheres will be counted).

2.11. Statistics

All statistical analyses were done in Origin Pro. All experiments were performed with at least n=6 samples per group, except for gene expression analysis which was performed with n=5 samples per group. Normality and equal variance were determined using Shapiro-Wilk and Brown-Forsythe, respectively. One-way ANOVA was used for normal data with equal variance followed by Tukey-HSD post-hoc analysis. A t-test with Welch correction was used for normal data without equal variance. Finally, Kruskal-Wallace with post-hoc analysis was

used for non-normal data. Significance reported for $p < 0.05$. All error bars reported are +/− standard error unless otherwise noted.

3. Results

3.1. Addition of zinc sulfate alters the morphology of the mineral phase

Scanning electron microscopy (SEM) analysis revealed that all scaffolds (Mineralized; 1X Zinc, 5X Zinc; 10X Zinc) displayed an open pore network (Fig. 1A). Stereology analysis revealed a minimal influence of zinc incorporation on scaffold pore size (Table 2), with the 10X Zinc scaffolds having significantly reduced pore size than the other scaffold variants. We subsequently examined the effect of zinc incorporation on the morphology of the resultant mineral content. The fabrication conditions for the mineralized collagen suspension result in the formation of a brushite mineral phase within the scaffold[14], under higher magnification the mineralized collagen scaffold control in this experiment exhibits the conventional plate-like mineral architecture of brushite mineral (Fig. 1B). However, incorporation of zinc ions leads to the formation of elongated, needle-like mineral precipitates, with crystal elongation increasing with increasing concentrations of zinc sulfate added to the precursor suspension (Fig. 1B).

3.2. Addition of zinc sulfate does not alter composition of the mineral phase

Due to the observed differences in the micron-scale morphology of the mineral deposits in the zinc functionalized scaffolds vs. the conventional mineralized collagen scaffold, we performed in depth compositional analysis of all scaffold variants. Despite the morphological differences, X-ray diffraction (XRD) indicates brushite is present in all scaffold variants (Fig. 2A). The XRD pattern associated with the zinc functionalized scaffolds is different from the pattern observed for pure zinc sulfate, and there are peaks present in the zinc sulfate spectra that are not present in the zinc functionalized scaffolds (Fig. 2B; red arrows). Further, unit cell analysis of brushite crystals within the scaffolds revealed the brushite lattice parameters (a, b, and c) as well as the beta angle of brushite (β=116.4°) do not deviate with increasing amounts of zinc sulfate (Fig. 2C).

3.3. Zinc-functionalized scaffolds can be tuned to alter mechanical properties and the release of zinc ions

We subsequently quantified the efficiency of zinc incorporation, the effect of zinc inclusion on scaffold mechanical properties, and release kinetics of zinc ions from the scaffold. Inductively coupled plasma mass spectrometry (ICP-MS) indicated that ~50% of zinc added to the mineralized collagen suspension was present in the freeze-dried scaffold (Fig. 2D).

Furthermore, the amount of calcium (Ca) and phosphorus (P) precipitated into the mineralized scaffold was not altered by the inclusion of zinc ions (Fig. 2E). Unconfined compression tests revealed that inclusion of zinc ions impacted scaffold elastic modulus, with 5X Zinc and 10X Zinc scaffolds showing significantly higher elastic modulus than the traditional mineralized and 1X Zinc scaffolds (Fig. 2F). The zinc ions incorporated into the scaffold mineral phase are released form the scaffold over extended culture, and this was previously observed for the calcium and phosphate components of the mineral phase [14].

ICP-MS analysis revealed steady release of zinc ions through 28 days in culture (37°C) into a model culture media (PBS + 1% BSA). This release was dependent on the dose of zinc incorporated into the scaffold (Fig. 3), with significant differences between all groups beginning at Day 4.

3.4. Zinc sulfate addition does not negatively impact cell activity at early time points

We subsequently examined the attachment and activity of porcine adipose derived stem cells (pASCs) within the zinc functionalized scaffold variants. We observed cell attachment and spreading on all scaffold variants after 7 days in culture (Fig. 4A, white arrowheads). We compared the number of attached pASCs and the metabolic activity of the cell seeded constructs over 7 days between groups to confirm that inclusion of zinc ions was not detrimental to stem cell activity. While there were some significant differences in cell number and metabolic activity between groups (notably increased metabolic activity for 5X and 10X Zinc scaffolds at Day 4), there was no significant differences in metabolic activity or cell number between groups by Day 7 (Fig. 4B). We decided to remove the 1X Zinc variant from subsequent long-term *in vitro* experiments because the metabolic activity observed for this group did not differ from the mineralized scaffold at any timepoint, the cell number for this group was lower than the mineralized scaffold at all timepoints, and there was no difference in elastic modulus when this group was compared to the mineralized scaffold.

3.4. Zinc functionalized scaffolds support long term pASC activity in vitro as well as signatures of osteogenic differentiation in the absence of osteogenic supplements

We subsequently performed an additional 8-week *in vitro* experiment, with cell-seeded scaffolds maintained in growth (not osteogenic) media. All scaffolds supported pASC proliferation and metabolic health. The 5X Zinc variant had the highest metabolic activity by Day 56 compared to the mineralized and 10X Zinc groups (Fig. 5A.) The 5X Zinc variant had the greatest pASC expansion, and this was especially noticeable at Days 14, 28, and 56 (Fig. 5B). Curiously, we observed a significant decrease in cell number after Day 7 in the 10X Zinc variant (Fig. 5B). This effect was not seen in the short term cell activity screen (Fig. 4); further, cell number and activity in the 10X Zinc variant rebounded by Day 56, and while not as strong as the 5x Zinc variant were consistent with results observed with our conventional mineralized collagen scaffold. Analysis of gene expression profiles displayed that all scaffold variants supported osteogenic activity of the seeded pASCs, despite the lack of osteogenic supplements (Fig. 6). Notably, zinc functionalized scaffolds supported increased levels of *COL1A2* (5X Zinc: Day 4), *BMP2* (10X Zinc: Day 1) and *RUNX2* (5X Zinc: Day 7). pASCs in zinc functionalized scaffolds also exhibited trends towards increased expression of the osteoblast-specific transcription factor OSTERIX (OSX; 5X Zinc: Days 4, 7; 10X Zinc: Days 1, 4, 7), the bone protein osteocalcin (*BGLAP:* 5X Zinc: Day 4; 10X Zinc: Days 1, 4, 7), and *BMP2* (5X Zinc: Days 1, 4; 10X Zinc: Day 4).

Interestingly, zinc functionalized scaffolds did not have increased expression of zinc transporters ZNT7, ZIP1, and ZIP13 compared to the mineralized scaffolds, except ZNT7 expression at Day 1 (Fig. 6). Additionally, there is an interesting trend in which ZNT7 expression increases until Day 7 in all scaffold variants and then decreases to Day 56 while

ZIP13 expression decreases until Day 7 in all scaffold variants and then increases to Day 56 (Supp. Fig. 3).

3.5. Zinc-functionalized scaffolds support new mineral deposition

In addition to metabolic health and gene expression, we evaluated the extent of mineral formation in pASC seeded scaffolds over the course of the 56-day experiment via micro-CT, comparing new mineral formation to unseeded scaffold controls (Fig. 7). Zinc functionalized scaffold controls had more and larger particles than mineralized scaffold controls at Day 0 (Fig. 7A–C). All scaffold had more particles at Day 28 and 56 compared to Day 0 controls (except for 5X Day 28 unseeded group) (Fig. 7B). We observed significantly more particles present in all scaffolds at Day 56 vs. to 28, showing mineral deposition over time. Further, 5X and 10X Zinc scaffolds contained more particles than unseeded controls by Day 56, though the particles were significantly smaller compared to Day 0 controls (Fig. 7C).

4. Discussion

This works builds on our recent development of a calcium phosphate mineralized collagen scaffold for craniomaxillofacial bone repair applications. Previously we have reported control over mineral weight percent (0–80%) and phase, pore size (100–250 μm), mechanical stiffness, and rate at which a portion of the calcium phosphate mineral is eluted from the scaffold as an osteogenic signal [16, 28, 34, 46, 47]. We identified a 40 weight percent calcium phosphate variant that promotes human mesenchymal stem cell osteogenic differentiation in the absence of osteogenic supplements (BMP-2, osteogenic media)[16, 46, 48, 49] as well as a mechanism for scaffold induced osteogenesis: activation of canonical (Smad1/5/8)[15] and Smad-independent (ERK½, Akt, p38 MAPK) BMP receptor signaling pathways[50]. While the mineralized collagen scaffold shows promising results in both in vitro osteogenesis and in vivo regeneration studies [18, 29], the inclusion of bioactive factors to further enhance osteogenesis and matrix production may be particularly important for large, geometrically complex craniomaxillofacial defects. Recently, studies begun to explore the use of mineral additives such as strontium and zinc to aid regenerative therapies for musculoskeletal injuries [51]. And with recent efforts examining the use of soluble zinc to aid osteogenesis [24, 52–54], including enhancing osteogenic differentiation of pASCs [26], here we examine incorporation of zinc ions into the mineral phase of a mineralized collagen scaffold and its influence on scaffold biophysical properties and pASC activity.

With the addition of zinc sulfate into the mineralized scaffolds, we did not observe a loss of the open pore network of the scaffold (Figure 1A) nor significant differences in mean pore size in the 1X and 5X Zinc variants (Table 2). However, we observed significant differences in the mineral microstructure, with zinc functionalized scaffolds presenting elongated crystal structures while traditional mineralized scaffolds present flattened, plate-like crystal structures commonly associated with brushite (Figure 1B). These findings inspire ongoing efforts to interrogate changes in cell interactions with elongated brushite crystallites, particularly their role in macrophage-scaffold interactions where material anisotropy may be instructive [55]. Interestingly, X-ray diffraction (XRD) analysis confirmed the mineral content of all scaffold variants was brushite (Figure 2A–B). Unit cell analysis confirmed

these findings, showing no change in brushite unit cell characteristics with increasing concentrations of zinc in the scaffold (Figure 2C). Zinc modified scaffolds (5X and 10X Zinc groups) also exhibited increased overall modulus (Fig. 2F); while moduli is reported for non-hydrated scaffolds we have previously shown that while hydration alters the absolute values of reported moduli it does not alter relative differences in moduli between groups [34, 40]. These data suggest the inclusion of sufficient zinc content (5x, 10x) can significantly enhance scaffold elastic modulus, although the role of the added zinc is unclear (overall increase in scaffold relative density, targeted effect of shifts in calcium phosphate morphology) and subject to future characterization. While the modulus of all scaffold variants is suboptimal for *in vivo* use, separate efforts by our group have described incorporating polymeric support frames into the scaffold to form a collagen-polymer composite with increased compressive strength [30, 56] and radial conformal fitting capabilities [56] that contribute to improved craniofacial bone repair in a Yorkshire pig mandible defect model [18].

We quantified the weight percent of zinc, calcium, and phosphorous incorporated into the freeze-dried scaffold structure (Figure 2D–E). We observed no relationship between incorporated zinc and the brushite weight percent (Figure 2E), suggesting the inclusion of zinc ions does not alter the amount of brushite precipitated into the scaffolds. Thus, observed differences in XRD peak intensity are likely a result of preferred crystal orientation, not brushite concentration. Plate-like and needle-like crystals result in different peak intensities due to differences in shape and direction of crystal growth. Together, these data suggest that the addition of zinc into our precursor suspension alters *how* brushite is precipitating within the scaffold. These morphological changes we see are consistent with work done by Madsen and Pederson, in which they tested the effects of metal ions on brushite formation [57, 58]. In this work they found that zinc was the only ion that caused aggregates of brushite to form, and these aggregates look like the brushite crystal morphology present in our freeze-dried zinc functionalized scaffolds. From our ICP-MS analysis, we observed approximately fifty percent of zinc added to the collagen suspension (across all zinc concentrations) was incorporated into the final scaffold (Figure 2D). Furthermore, we observed zinc release curves from the mineralized collagen scaffolds that showed dose-dependence (Fig. 3). Interestingly, we created zinc scaffold variants with the goal of matching ion concentrations near the 0.04mM concentration recently identified by Bertels *et al.* to promote pASC osteogenesis in 2D tissue culture [26]. We calculated the amount of zinc included into our scaffolds based on previous efforts that characterize release of calcium and phosphate ions from the mineralized collagen scaffold [14]. While the observed zinc release in this experiment was below this target, we still observed an influence of zinc on enhanced pASC metabolic activity and cell number, setting the stage for future efforts to identify an optimal range for zinc inclusion into three-dimensional scaffolds for bone repair.

A critical finding from this work is that zinc incorporation does not have negative consequences on porcine adipose derived stem cell (pASC) activity. pASCs have previously been shown to have strong osteoinductive properties [41, 59–62], making them intriguing targets for craniofacial bone repair applications. pASCs were able to attach and spread on all scaffold variants (Figure 4A), with no significant differences with the addition of zinc ions. Further, we observed no short-term negative consequences in terms of altered metabolic

activity or cell number due to the incorporation of zinc at any tested dose (Figure 4B). Due to the low concentration of released zinc, largely similar short-term cell response compared to the mineralized scaffold, and the less robust elongated zinc deposits in the 1X zinc variant (Supp. Fig. 1), we chose to remove this group from the extended (8-week) cell activity experiment. Over an elongated culture period, the 5X zinc scaffold group displayed the highest metabolic activity and cell number by Day 56. The 5X Zinc variants had the highest metabolic activity as early as Day 7, with significant differences occurring by Day 28 (Figure 5). High cell number and increased metabolic activity are important for clinical applications, because we want to see cell proliferation quickly in our defect area in addition to high cell metabolic activity.

Analysis of gene expression profiles across the extended culture reveal a signature that zinc modified scaffolds support pASC osteogenesis. Genes important for bone remodeling and osteogenesis (i.e. all genes besides the zinc transporters – ZNT7, ZIP1, and ZIP13) were upregulated at all timepoints, indicating addition of zinc does not negatively impacting the cells ability to deposit collagen matrix and early osteoblast differentiation [63–65]. Examining zinc transporters, we observed that as ZNT7 expression decreased after Day 7, ZIP13 expression increased, consistent with previous finding that ZnTs decrease cytosolic zinc concentrations while ZIPs increase cytosolic zinc concentrations [66]. Higher expression of ZIP1 and ZIP13 in mineralized and 5X zinc scaffolds suggests cells are trying to transport zinc into their cytosol. With the highest ZnT7 in 10X and 5X Zinc variants, cells are likely decreasing their cytosolic zinc content at earlier timepoints as compared to cells within conventional mineralized scaffolds. These finding motivate future study of a larger selection of zinc transporters via both PCR and Western Blot which would provide more information about the zinc transport in our zinc functionalized scaffolds. While recent work using pASCs shows the osteogenic benefit of zinc ions motivated this study to examine the behavior of pASCs on zinc-functionalized scaffolds, the relative difficulty of finding porcine PCR primers and Western Blot antibodies motivate future studies to examine the role of zinc-functionalized scaffolds using human mesenchymal stromal cells and examining the broad array of identified zinc transporters in human cells [66].

Analysis of mineral deposits via microcomputed tomography (micro-CT) showed increasing number of mineral deposits for all scaffold variants from Day 28 to 56. However, the sizes of particles shifted substantially, with increasing particle size for mineralized scaffolds but decreasing in zinc functionalized scaffolds (relative to Day 0 control). Drivers for changes in particle size include cell mediated deposition, but also shifts due to the release of mineral from the scaffold. Previous studies of mineralized scaffolds showed significant release of Ca and P ions from the scaffolds [16]. Given the particle size of zinc functionalized scaffolds was significantly different (needle-like deposits vs. conventional Brushite plates), the challenge of comparing overall changes in mineral particle size as a function of time (and mineral release) is difficult. While this work focuses on the development and thorough characterization of a novel class of zinc functionalized mineralized collagen scaffolds for craniofacial bone regeneration application, an important future stage of this work is in depth *in vivo* analysis of bone repair. We have recently completed initial evaluation of bone regeneration induced via the mineralized collagen scaffolds using both a rabbit calvarial defect [29] and a porcine mandible defect model [18]. In these models the mineralized

collagen scaffold promoted robust bone regeneration, and we identified a role for the scaffold in both promoting osteogenic differentiation and bone synthesis but also acting to inhibit osteoclast activity [67, 68]. The enhanced cell activity identified within zinc-functionalized mineralized collagen scaffolds suggest that an essential next step for these materials is functional assessment via these robust preclinical models.

5. Conclusions

A key challenge for biomaterials designed for craniomaxillofacial bone regeneration is the capacity to promote robust osteoinduction, biomaterial driven cell recruitment, osteogenic differentiation, and new matrix biosynthesis. Here we report modification of a mineralized collagen scaffold under development for craniomaxillofacial bone repair via inclusion of zinc ions as an osteogenic supplement. We report the effects of zinc supplementation on scaffold biophysical and compositional properties as well as the results of *in vitro* cell activity experiments. Notably, zinc-functionalized scaffolds retain the brushite phase of calcium phosphate mineral, but displayed altered mineral microstructure, increased elastic moduli, and with in vitro testing reveal the zinc-functionalized scaffold can enhanced the overall number and cell metabolic activity of pASCs seeded within the scaffold. Together, these findings suggest the zinc-functionalized mineralized collagen scaffold provides a biomaterial platform to investigate in vitro the role of zinc inclusion on osteogenic signal transduction via calcium and zinc ion transporters as well as to examine new bone formation via a series of established porcine and rabbit craniofacial bone defect models.

Supplementary Material

Refer to Web version on PubMed Central for supplementary material.

Acknowledgements

The authors acknowledge Dr. Matthew Wheeler (U. Illinois) for the gift of porcine derived adipose stems cells. This work was supported by the Office of the Assistant Secretary of Defense for Health Affairs Broad Agency Announcement for Extramural Medical Research through the Award No. W81XWH-16–1-0566. Opinions, interpretations, conclusions and recommendations are those of the authors and are not necessarily endorsed by the Department of Defense. Research reported in this publication was also supported by the National Institute of Dental and Craniofacial Research of the National Institutes of Health under Award Number R21 DE026582. The content is solely the responsibility of the authors and does not necessarily represent the official views of the NIH. We are grateful for the funding for this study provided by the NSF Graduate Research Fellowship DGE-1144245 (AST).

The authors would like to acknowledge the University of Illinois Roy J. Carver Biotechnology Center for assistance with real-time PCR. The authors also acknowledge assistance from the School of Chemical Science Microanalysis Lab for assistance with inductively coupled plasma mass spectrometry/optical emission spectrometry and the George L. Clark S-Ray Facility and 3M Materials laboratory for assistance with x-ray diffraction and unit cell analysis. This research was carried out in part at the Imaging Technology Group within the Beckman Institute for Advanced Science and Technology at the University of Illinois at Urbana-Champaign. The authors would like to thank Leilei Yin for help with microcomputed tomography, as well as Scott Robinson and Cate Wallace for assistance with critical point drying and scanning electron microscopy. Additional support was provided by the Chemical and Biomolecular Engineering Dept. and the Carl R. Woese Institute for Genomic Biology (BACH) at the University of Illinois at Urbana-Champaign.

References

[1]. Hussain K, Wijetunge DB, Grubnic S, Jackson I. A comprehensive analysis of craniofacial trauma. The Journal of Trauma 1994;36:14.

[2]. Rajendra PB, Mathew TP, Agrawal A, Sabharawal G. Characteristics of associated craniofacial trauma in patients with head injuries: An experience with 100 cases. J Emerg Trauma Shock 2009;2:89–94. [PubMed: 19561967]

[3]. Carvalho TBO, Cancian LRL, Marques CG, Piatto B, Maniglia JV, Molina FD. Six years of facial trauma care, an epidemilogical analysis of 355 cases. Brazilian Journal of Otorhinolaryngology 2010;76:10.

[4]. Owens BD, Kragh JF Jr., Wenke JC, Macaitis J, Wade CE, Holcomb JB. Combat wounds in operation Iraqi Freedom and operation Enduring Freedom. J Trauma 2008;64:295–9. [PubMed: 18301189]

[5]. Lew TA, Walker JA, Wenke JC, Blackbourne LH, Hale RG. Characterization of craniomaxillofacial battle injuries sustained by United States service members in the current conflicts of Iraq and Afghanistan. J Oral Maxillofac Surg 2010;68:3–7. [PubMed: 20006147]

[6]. Hale RG, Hayes DK, Orloff G, Peterson K, Powers DB, Mahadevan S. Maxillofacial and Neck Trauma.

[7]. Thompson EM, Matsiko A, Farrell E, Kelly DJ, O'Brien FJ. Recapitulating endochondral ossification: a promising route to in vivo bone regeneration. J Tissue Eng Regen Med 2015;9:889–902. [PubMed: 24916192]

[8]. Zimmermann G, Moghaddam A. Allograft bone matrix versus synthetic bone graft substitutes. Injury 2011;42:S16–21. [PubMed: 21889142]

[9]. Laurencin C, Khan Y, El-Amin SF. Bone graft substitutes. Expert Rev Med Devices 2006;3:49–57. [PubMed: 16359252]

[10]. Lorenz J, Schlee M, Al-Maawi S, Chia P, Sader RA, Ghanaati S. Variant Purification of an Allogeneic Bone Block. Acta Stomatol Croat 2017;51:141–7. [PubMed: 28827851]

[11]. Lynn AK, Best SM, Cameron RE, Harley BA, Yannas IV, Gibson LJ, Bonfield W. Design of a multiphase osteochondral scaffold I: control of chemical composition. J Biomed Mater Res A 2010;92:1057–65. [PubMed: 19301264]

[12]. Quinlan E, Lopez-Noriega A, Thompson E, Kelly HM, Cryan SA, O'Brien FJ. Development of collagen-hydroxyapatite scaffolds incorporating PLGA and alginate microparticles for the controlled delivery of rhBMP-2 for bone tissue engineering. J Control Release 2015;198:71–9. [PubMed: 25481441]

[13]. David F, Levingstone TJ, Schneeweiss W, de Swarte M, Jahns H, Gleeson JP, O'Brien FJ. Enhanced bone healing using collagen-hydroxyapatite scaffold implantation in the treatment of a large multiloculated mandibular aneurysmal bone cyst in a thoroughbred filly. Journal of Tissue Engineering and Regenerative Medicine 2015:n/a–n/a.

[14]. Weisgerber DW, Caliari SR, Harley BA. Mineralized collagen scaffolds induce hMSC osteogenesis and matrix remodeling. Biomater Sci 2015;3:533–42. [PubMed: 25937924]

[15]. Ren X, Bischoff D, Weisgerber DW, Lewis MS, Tu V, Yamaguchi DT, Miller TA, Harley BA, Lee JC. Osteogenesis on nanoparticulate mineralized collagen scaffolds via autogenous activation of the canonical BMP receptor signaling pathway. Biomaterials 2015;50:107–14. [PubMed: 25736501]

[16]. Weisgerber DW, Caliari SR, Harley BAC. Mineralized collagen scaffolds induce hMSC osteogenesis and matrix remodeling. Biomater Sci 2015;3:533–42. [PubMed: 25937924]

[17]. Ren X, Weisgerber DW, Bischoff D, Lewis MS, Reid RR, He TC, Yamaguchi DT, Miller TA, Harley BA, Lee JC. Nanoparticulate Mineralized Collagen Scaffolds and BMP-9 Induce a Long-Term Bone Cartilage Construct in Human Mesenchymal Stem Cells. Adv Healthc Mater 2016;5:1821–30. [PubMed: 27275929]

[18]. Weisgerber DW, Milner DJ, Lopez-Lake H, Rubessa M, Lotti S, Polkoff K, Hortensius RA, Flanagan CL, Hollister SJ, Wheeler MB, Harley BAC. A mineralized collagen-polycaprolactone composite promotes healing of a porcine mandibular ramus defect. Tissue Eng Part A 2018;24:943–54. [PubMed: 29264958]

[19]. Ren X, Tu V, Bischoff D, Weisgerber DW, Lewis MS, Yamaguchi DT, Miller TA, Harley BA, Lee JC. Nanoparticulate mineralized collagen scaffolds induce in vivo bone regeneration independent of progenitor cell loading or exogenous growth factor stimulation. Biomaterials 2016;89:67–78. [PubMed: 26950166]

[20]. Haumont S distribution of zinc in bone tissue. 1960:5.

[21]. Keith A McCall C-cH, Fierke Carol A.. Function and Mechanism of Zinc Metalloenzymes. The Journal of Nutrition 2000;130:10. [PubMed: 10613758]

[22]. Hojyo S, Fukada T, Shimoda S, Ohashi W, Bin BH, Koseki H, Hirano T. The zinc transporter SLC39A14/ZIP14 controls G-protein coupled receptor-mediated signaling required for systemic growth. PLoS One 2011;6:e18059. [PubMed: 21445361]

[23]. Prasad ASSA, Miale A Jr, Farid Z, Sandstead HH. Zinc and Iron Deficiencies in Male Subjects with Dwarfism and Hypogonadism but Without Ancylostomiasis, Schistosomiasis or Severe Anemia. American Journal of Clinical Nutrition 1963;12:8.

[24]. Yusa K, Yamamoto O, Iino M, Takano H, Fukuda M, Qiao Z, Sugiyama T. Eluted zinc ions stimulate osteoblast differentiation and mineralization in human dental pulp stem cells for bone tissue engineering. Arch Oral Biol 2016;71:162–9. [PubMed: 27521529]

[25]. An S, Gong Q, Huang Y. Promotive Effect of Zinc Ions on the Vitality, Migration, and Osteogenic Differentiation of Human Dental Pulp Cells. Biol Trace Elem Res 2017;175:112–21. [PubMed: 27260533]

[26]. Bertels JC, Rubessa M, Schreiber SR, Wheeler MB. The effect of zinc on the differentiation of adipose-derived stem cells into osteoblasts. Reproduction, fertility, and development 2016;29:207.

[27]. Zhou Q, Ren X, Bischoff D, Weisgerber DW, Yamaguchi DT, Miller TA, Harley BAC, Lee Jc. Nonmineralized and mineralized collagen scaffolds induce differential osteogenic signaling pathways in human mesenchymal stem cells. Advanced healthcare materials 2017;6:1700641.

[28]. Harley BA, Lynn AK, Wissner-Gross Z, Bonfield W, Yannas IV, Gibson LJ. Design of a multiphase osteochondral scaffold II: fabrication of a mineralized collagen-GAG scaffold. J Biomed Mater Res A 2010;92:1066–77. [PubMed: 19301274]

[29]. Ren X, Tu V, Bischoff D, Weisgerber DW, Lewis MS, Yamaguchi DT, Miller TA, Harley BAC, Lee JC. Nanoparticulate mineralized collagen scaffolds induce in vivo bone regeneration independent of progenitor cell loading or exogenous growth factor stimulation. Biomaterials 2016;89:67–78. [PubMed: 26950166]

[30]. Weisgerber DW, Erning K, Flanagan CL, Hollister SJ, Harley BAC. Evaluation of multi-scale mineralized collagen-polycaprolactone composites for bone tissue engineering. J Mech Behav Biomed Mater 2016;61:318–27. [PubMed: 27104930]

[31]. Grier WK, Tiffany AS, Ramsey MD, Harley BAC. Incorporating β-cyclodextrin into collagen scaffolds to sequester growth factors and modulate mesenchymal stem cell activity. Acta Biomaterialia 2018;76:116–25. [PubMed: 29944975]

[32]. Caliari SR, Harley BA. The effect of anisotropic collagen-GAG scaffolds and growth factor supplementation on tendon cell recruitment, alignment, and metabolic activity. Biomaterials 2011;32:5330–40. [PubMed: 21550653]

[33]. O'Brien FJ, Harley BA, Yannas IV, Gibson L. Influence of freezing rate on pore structure in freeze-dried collagen-GAG scaffolds. Biomaterials 2004;25:1077–86. [PubMed: 14615173]

[34]. Weisgerber DW, Kelkhoff DO, Caliari SR, Harley BAC. The impact of discrete compartments of a multi-compartment collagen-GAG scaffold on overall construct biophysical properties. J Mech Behav Biomed Mater 2013;28:26–36. [PubMed: 23973610]

[35]. O'Brien FJ, Harley BA, Yannas IV, Gibson LJ. The effect of pore size on cell adhesion in collagen-GAG scaffolds. Biomaterials 2005;26:433–41. [PubMed: 15275817]

[36]. Gibson LJ, Ashby MF. Cellular solids: structure and properties. 2nd ed. Cambridge, U.K.: Cambridge University Press; 1997.

[37]. Kanungo BP, Gibson LJ. Density-property relationships in collagen-glycosaminoglycan scaffolds. Acta Biomater 2009;6:344–53. [PubMed: 19770077]

[38]. Kanungo BP, Gibson LJ. Density-property relationships in mineralized collagen-glycosaminoglycan scaffolds. Acta Biomater 2009;5:1006–18. [PubMed: 19121982]

[39]. Kanungo BP, Silva E, Van Vliet K, Gibson LJ. Characterization of mineralized collagen-glycosaminoglycan scaffolds for bone regeneration. Acta Biomater 2008;4:490–503. [PubMed: 18294943]

[40]. Harley BA, Leung JH, Silva EC, Gibson LJ. Mechanical characterization of collagen-glycosaminoglycan scaffolds. Acta Biomater 2007;3:463–74. [PubMed: 17349829]

[41]. Monaco E, Bionaz M, Rodriguez-Zas S, Hurley WL, Wheeler MB. Transcriptomics comparison between porcine adipose and bone marrow mesenchymal stem cells during in vitro osteogenic and adipogenic differentiation. PLoS ONE 2012;7:e32481. [PubMed: 22412878]

[42]. Caliari SR, Ramirez MA, Harley BAC. The development of collagen-GAG scaffold-membrane composites for tendon tissue engineering. Biomaterials 2011;32:8990–8. [PubMed: 21880362]

[43]. Caliari SR, Grier WK, Weisgerber DW, Mahmassani Z, Boppart MD, Harley BAC. Collagen scaffolds incorporating coincident gradations of instructive structural and biochemical cues for osteotendinous junction engineering. Advanced healthcare materials 2015;4:831–7. [PubMed: 25597299]

[44]. Shanbhag AG. Utilization of Information Measure as a Means of Image Thresholding. Graphical Models and Image Processing 1994;56:6.

[45]. Mehmet Sezgin BlS. Survey over image thresholding techniques and quantitative performance evaluation. Journal of Electronic Imaging 2004;13:23.

[46]. Caliari SR, Harley BAC. Structural and biochemical modification of a collagen scaffold to selectively enhance MSC tenogenic, chondrogenic, and osteogenic differentiation. Advanced healthcare materials 2014;3:1086–96. [PubMed: 24574180]

[47]. Lee JC, Pereira CT, Ren X, Huang W, Weisgerber DW, Yamaguchi DT, Harley BAC, Miller TA. Optimizing collagen scaffolds for bone engineering: effects of crosslinking and mineral content on structural contraction and osteogenesis. J Craniofac Surg 2015;26:1992–6. [PubMed: 26147021]

[48]. Caliari SR, Harley BAC. Collagen-GAG scaffold biophysical properties bias MSC lineage selection in the presence of mixed soluble signals. Tissue Eng A 2014;20:2463–72.

[49]. Banks JM, Mozdzen LC, Harley BAC, Bailey RC. The combined effects of matrix stiffness and growth factor immobilization on the bioactivity and differentiation capabilities of adipose-derived stem cells. Biomaterials 2014;35:8951–9. [PubMed: 25085859]

[50]. Ren X, Weisgerber DW, Bischoff D, Lewis MS, Reid RR, He T-c, Yamaguchi DT, Miller TA, Harley BAC, Lee JC. Nanoparticulate mineralized collagen scaffolds and BMP-9 induce a long term bone cartilage construct in human mesenchymal stem cells. Advanced healthcare materials 2016;5:1821–30. [PubMed: 27275929]

[51]. Jiménez M, Abradelo C, San Román J, Rojo L. Bibliographic review on the state of the art of strontium and zinc based regenerative therapies. Recent developments and clinical applications. J Mater Chem B Mater Biol Med 2019;7:1974–85.

[52]. Ghasemzadeh-Hasankolai M, Batavani R, Eslaminejad MB, Sedighi-Gilani M. Effect of zinc ions on differentiation of bone marrow-derived mesenchymal stem cells to male germ cells and some germ cell-specific gene expression in rams. Biological trace element research 2012;150:137–46. [PubMed: 22890879]

[53]. Yusa K, Yamamoto O, Fukuda M, Koyota S, Koizumi Y, Sugiyama T. In vitro prominent bone regeneration by release zinc ion from Zn-modified implant. Biochemical and Biophysical Research Communications 2011;412:273–8. [PubMed: 21820411]

[54]. Oh SA, Kim SH, Won JE, Kim JJ, Shin US, Kim HW. Effects on growth and osteogenic differentiation of mesenchymal stem cells by the zinc-added sol-gel bioactive glass granules. Journal of tissue engineering 2011;2010:475260. [PubMed: 21350651]

[55]. McWhorter FY, Wang T, Nguyen P, Chung T, Liu WF. Modulation of macrophage phenotype by cell shape. Proc Natl Acad Sci U S A 2013;110:17253–8. [PubMed: 24101477]

[56]. Dewey MJ, Johnson EM, Weisgerber DW, Wheeler MB, Harley BAC. Shape-fitting collagen-PLA composite promotes osteogenic differentiation of porcine adipose stem cells. J Mech Behav Biomed Mater 2019.

[57]. Lundager Mades HE, Pederson JB. Influence of foreign metal ions on crystal morphology and transformation of brushite. Advances in Crystal Growth Inhibition Technologies 2002:13.

[58]. Lundager Madsen HE. Influence of foreign metal ions on crystal growth and morphology of brushite (CaHPO4, 2H2O) and its transformation to octacalcium phosphate and apatite. J Cryst Growth 2008;310:2602–12.

[59]. Wilson SM, Goldwasser MS, Clark SG, Monaco E, Bionaz M, Hurley WL, Rodriguez-Zas S, Feng L, Dymon Z, Wheeler MB. Adipose-derived mesenchymal stem cells enhance healing of mandibular defects in the ramus of swine. J Oral Maxillofac Surg 2012;70:e193–203. [PubMed: 22374062]

[60]. Monaco E, Bionaz M, Hollister SJ, Wheeler MB. Strategies for regeneration of the bone using porcine adult adipose-derived mesenchymal stem cells. Theriogenology 2011;75:1381–99. [PubMed: 21354606]

[61]. Kim D, Monaco E, Maki A, de Lima AS, Kong HJ, Hurley WL, Wheeler MB. Morphologic and transcriptomic comparison of adipose- and bone-marrow-derived porcine stem cells cultured in alginate hydrogels. Cell Tissue Res 2010;341:359–70. [PubMed: 20680346]

[62]. Monaco E, Lima AS, Bionaz M, Maki A, Wilson Sm, Hurley WL, Wheeler MB. Morphological and transcriptomic comparison of adipose and bone marrow derived porcine stem cells. Open Tiss Eng Regen Med J 2009;2.

[63]. Marsell R, Einhorn TA. The biology of fracture healing. Injury 2011;42:551–5. [PubMed: 21489527]

[64]. Le BQ, Nurcombe V, Cool SM, van Blitterswijk CA, de Boer J, LaPointe VLS. The Components of Bone and What They Can Teach Us about Regeneration. Materials (Basel) 2017;11.

[65]. Schell H, Duda GN, Peters A, Tsitsilonis S, Johnson KA, Schmidt-Bleek K. The haematoma and its role in bone healing. J Exp Orthop 2017;4:5. [PubMed: 28176273]

[66]. Bafaro E, Liu Y, Xu Y, Dempski RE. The emerging role of zinc transporters in cellular homeostasis and cancer. Signal Transduct Target Ther 2017;2.

[67]. Ren X, Zhou Q, Foulad D, Dewey MJ, Miller TA, Yamaguchi DT, Bischoff D, Harley BAC, Lee JC. Nanoparticulate mineralized collagen glycosaminoglycan materials directly and indirectly inhibit osteoclastogenesis and osteoclast activation. J Tissue Eng Regen Med 2019.

[68]. Ren X, Zhou Q, Foulad D, Tiffany AS, Dewey MJ, Bischoff D, Miller TA, Reid RR, He T-c, Yamaguchi DT, Harley BAC, Lee JC. Osteoprotegerin reduces osteoclast resorption activity without affecting osteogenesis on nanoparticulate mineralized collagen glycosaminoglycan scaffolds. Sci Adv 2019.

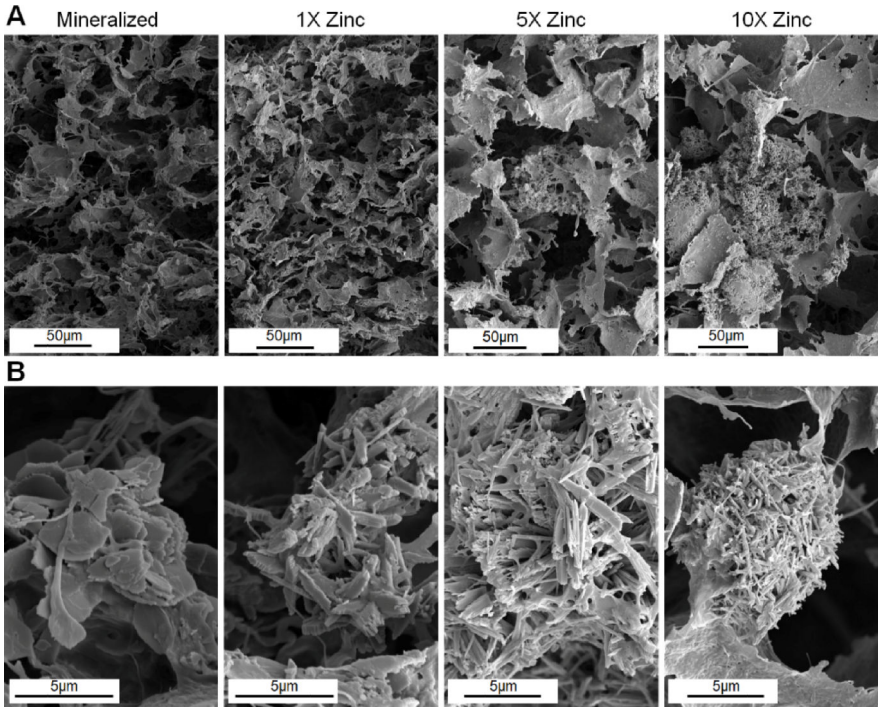

Figure 1: Scanning electron microscopy images of mineralized zinc scaffolds show alterations in crystal microstructure.

(A) There are no noticeable changes to pore structure across scaffold variants, but there are noticeable changes in crystal aggregates in 5X and 10X zinc groups. **(B)** The addition of zinc alters the brushite microstructure within the scaffolds from plate-like crystals to elongated needle-like structures. (Top: Magnifications – 800X, 800X, 600X, 600X; Bottom: Magnifications – 12,000X, 12,000X, 10,000X, 8000X; 16-bit Tiff images; Cropped to size only).

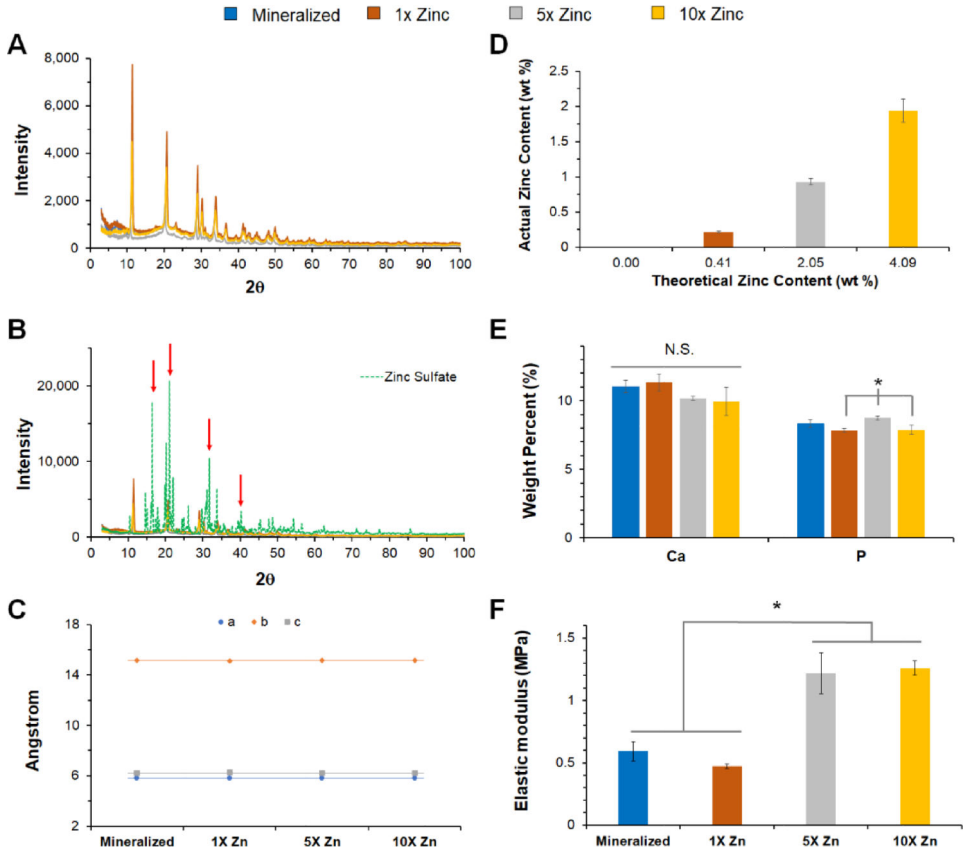

Figure 2: Compositional and mechanical analysis of zinc-functionalized mineralized scaffolds.

(A) X-ray diffraction patterns of mineralized and zinc functionalized scaffolds indicate brushite is present in all variants. **(B)** X-ray diffraction data from 2A overlaid with zinc sulfate diffraction pattern. Additional peaks present in zinc sulfate are not present in zinc functionalized scaffolds (red arrows). **(C)** Unit cell analysis of brushite within each scaffold variant, indicating that increasing zinc concentration does not change unit cell parameters. **(D)** ICP-MS analysis of zinc in scaffolds. Approximately 50% of zinc added into slurry is in scaffolds. All groups are significantly different from one another at $p<0.05$. **(E)** ICP-OES analysis of calcium and phosphorus content in each scaffold demonstrate no relationship between inclusion of zinc and the overall amount of calcium phosphate in the scaffold. **(F)** Elastic modulus for each scaffold variant. *: significance reported at $p<0.05$.

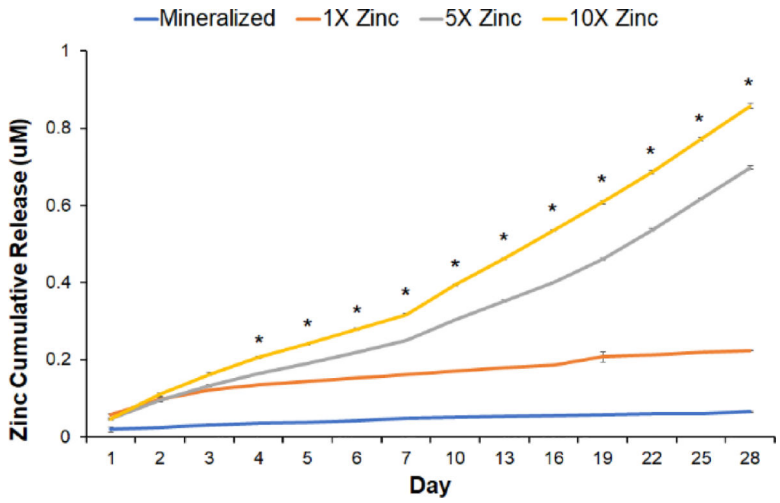

Figure 3: Zinc ion release.

Zinc ion release quantified using ICP-MS for all scaffold variants: Mineralized, 1X Zinc, 5X Zinc, and 10X Zinc. *: significance between all groups reported at $p<0.05$.

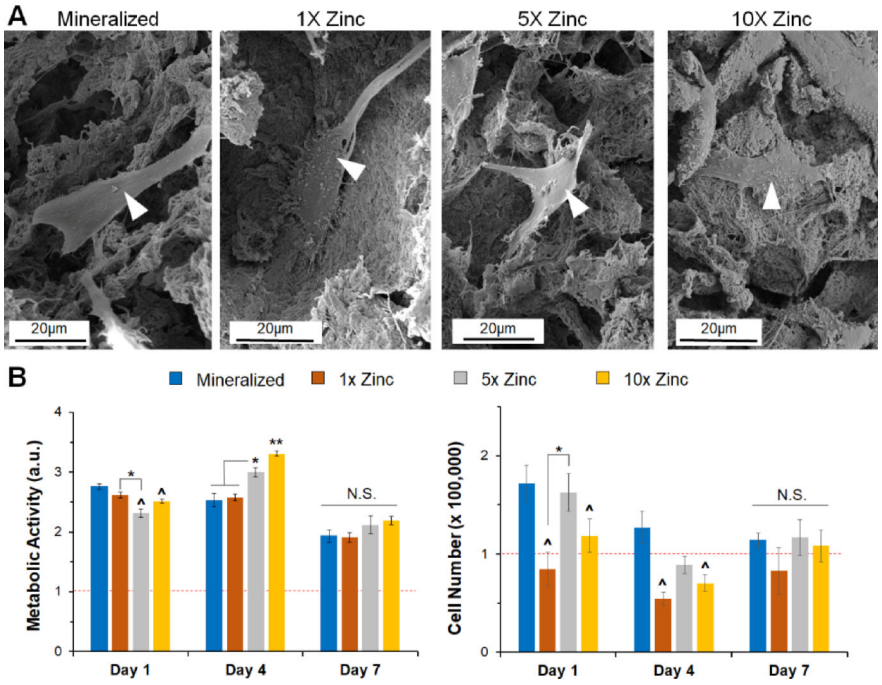

Figure 4: Short-term cell morphology and activity on mineralized and zinc scaffolds.

(A) SEM images of seeded scaffolds show healthy cell spreading and morphology on all variants. **(B)** Metabolic activity for porcine derived adipose stem cells on all scaffold variants. No significant differences were seen between mineralized and 1X zinc groups for any timepoint. **(C)** Cell number showed no significance impact of zinc concentration on cell number by Day 7. (Magnifications – 2,400X, 2,500X, 2,400X, 2,500X; 16-bit Tiff images; Cropped to size only). *: significance at $p<0.05$ for indicated groups. ^: significance at $p<0.05$ compared to mineralized scaffold. **: significant at $p<0.05$ compared to all groups. N.S.: no significance between indicated groups.

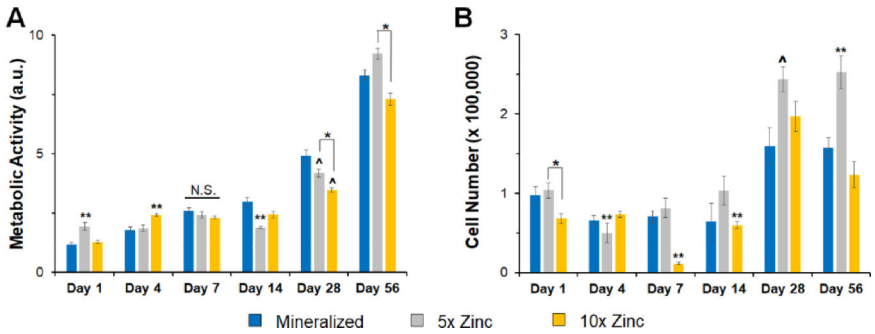

Figure 5: Long-term cell metabolic activity and cell number.

(A) Metabolic activity of pASCs showing the 5X Zinc variant has the highest cell activity at Day 56. **(B)** Overall number of attached pASCs showing the 5X Zinc variant has the highest cell number starting at Day 7, becoming significant by Day 28. *: significance at $p<0.05$ for indicated groups. ^: significance at $p<0.05$ compared to mineralized scaffold. **: significant at $p<0.05$ compared to all groups. N.S.: no significance between indicated groups.

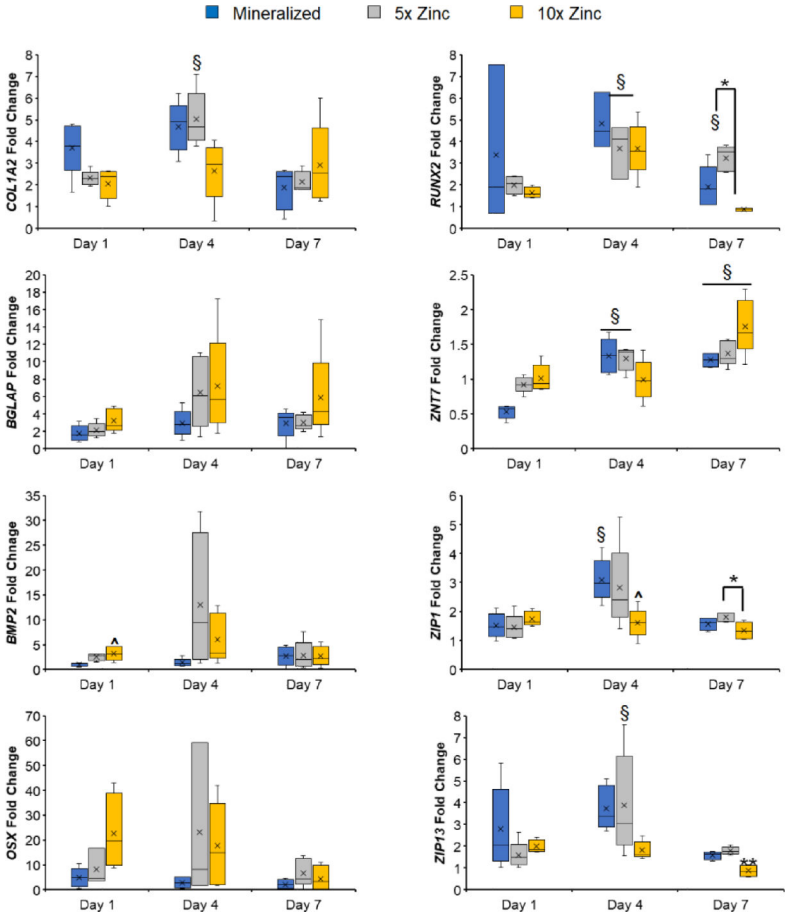

Figure 6: Gene expression profiles for osteogenesis and zinc transporters.

All scaffolds display upregulated genes related to osteogenesis – COL1A2, BGLAP, BMP2, OSX, and RUNX2 – and more dynamic expression profiles of zinc transporters – ZNT7, ZIP1, and ZIP13. See Supplemental Figure 2 for long-term gene expression profiles. ^: significance at $p<0.05$ for indicated groups. ^: significance at $p<0.05$ compared to mineralized scaffold. **: significant at $p<0.05$ compared to all groups. N.S.: no significance between indicated groups. #: significant ($p<0.05$) decrease compared to Day 1 within experimental group. §: significant ($p<0.05$) increase compared to Day 1 within experimental group.

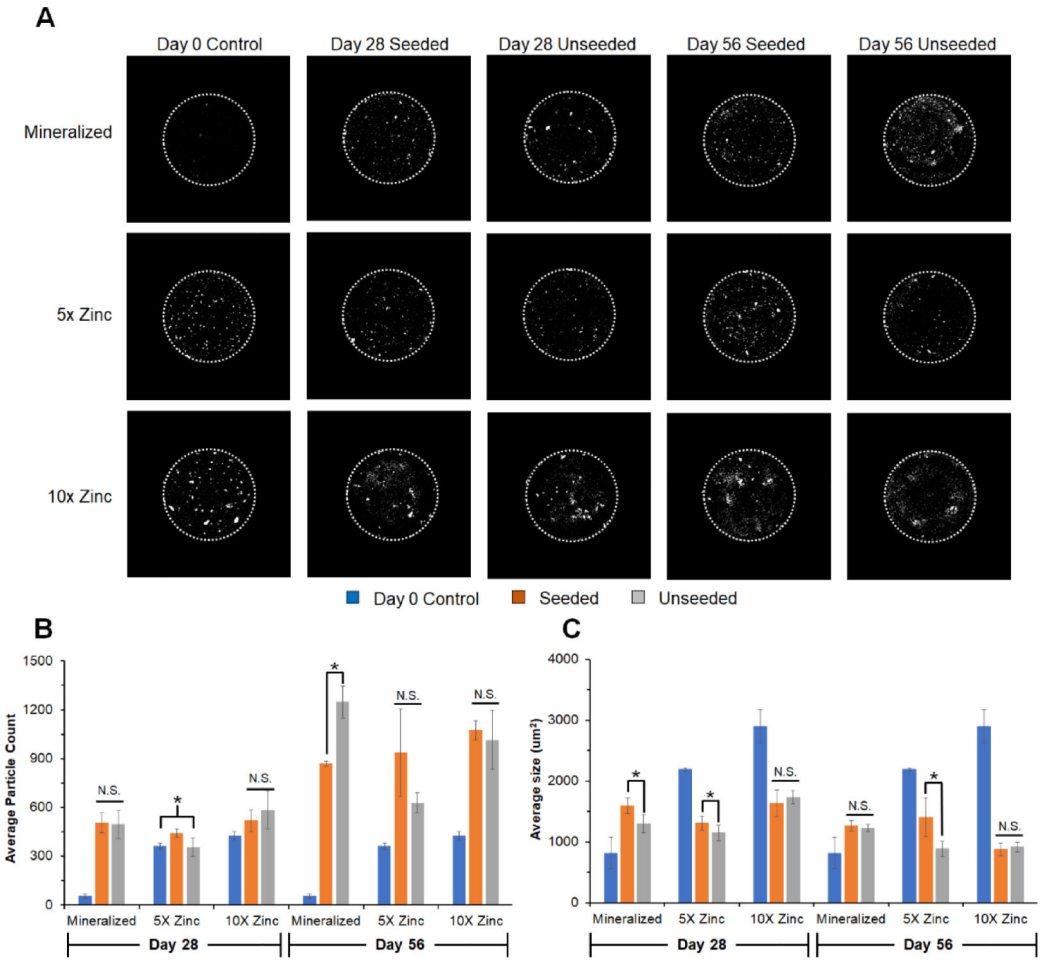

Figure 7: Micro-CT analysis of mineral remodeling over longe-term in vitro culture.

(A) Representative images (middle slice from each image stack) of mineralized, 1X Zinc, and 5X Zinc scaffolds along with unseeded controls. Diameter of scaffold is 6mm (dotted white line). **(B)** Average particle count representative of mineral nodules apparent within the scaffold. Overall, number of nodules increased from Day 28 to Day 56. All groups had significantly more particles than the unseeded Day 0 controls by Day 56. **(C)** Average particle size within scaffolds, showing mineralized scaffolds display larger particles compared to their unseeded Day 0 controls while the zinc functionalized scaffolds display significantly smaller particles compared to their unseeded Day 0 controls. *: significance at $p<0.05$ for indicated groups. N.S.: no significance between indicated groups.

Table 1.

PCR primers and supplier.

Transcript	Supplier	Assay ID
GAPDH	ThermoFisher (Taqman)	Ss03375629_u1
COL1A2	ThermoFisher (Taqman)	Ss03375009_u1
BGLAP	ThermoFisher (Taqman)	Ss03373655_s1
BMP2	ThermoFisher (Taqman)	Ss03373798_g1
OSTERIX	ThermoFisher (Taqman)	Ss03373734_s1
ZNT7	ThermoFisher (Taqman)	Ss03819782_s1
GAPDH	Bio-Rad (SYBR Green)	qSscCED0017494
RUNX2	Bio-Rad (SYBR Green)	qSscCID0002170
ZIP1	Bio-Rad (SYBR Green)	qSscCED0016809
ZIP13	Bio-Rad (SYBR Green)	qSscCED0011005

Table 2.

Pore size of zinc functionalized scaffold normalized to mineralized scaffolds (62 ± 1 μm).

	Mineralized	1x Zinc	5x Zinc	10x Zinc
Normalized Pore Diameter	1.00	0.93	0.98	0.85
Standard Error (±)	0.02	0.01	0.02	0.01